Establishment of correlations for the thermo-hydraulic parameters due to perforation in a multi-V rib roughened single pass solar air heater

Varun Pratap Singh, Siddharth Jain & Ashwani Kumar

Published online: 18 Apr 2022.

Submit your article to this journal ☑

View related articles ☑

View Crossmark data ☑

Taylor & Francis
Taylor & Francis Group

Check for updates

Establishment of correlations for the thermo-hydraulic parameters due to perforation in a multi-V rib roughened single pass solar air heater

Varun Pratap Singh [ID][a], Siddharth Jain [ID][b], and Ashwani Kumar[c]

[a]Department of Mechanical Engineering, School of Engineering, University of Petroleum and Energy Studies, Energy Acres, Bidholi, Dehradun, 248007, India; [b]Department of Mechanical Engineering, College of Engineering Roorkee (COER), Roorkee, India; [c]Technical Education Department Uttar Pradesh, Kanpur India

ABSTRACT

The effect of variation in open area ratio (β) in a multi-V rib roughened Single-Pass Solar Air Heater (SPSAH) is analyzed in this work. Fixing values of other parameters, such as open area ratio (β) and relative roughness width (W/w), were studied with a certain range of Reynolds number (Re) ranging from 2000 to 18000. The improvement in Nusselt number ratio (Nu/Nus) and thermo-hydraulic performance (THPP) and the decline in duct friction ratio (f/fs) support the application of perforation. The empirical correlations of Nu and f are also generated with ±12% and ±7.5% accuracy.
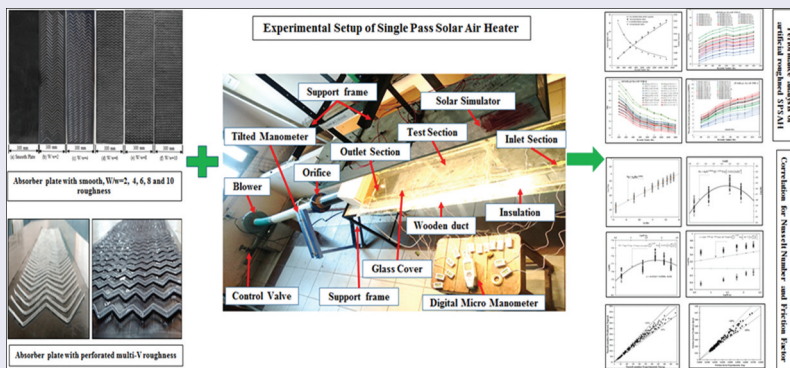
Introduction

Solar, wind, hydro, tidal, geothermal, and biomass energy are now the most common renewable energy sources [1–3]. Due to large availability and high level of acceptability solar energy having larger applications in domestic and commercial uses either in thermal and photvoltic conversion [4]. A Solar Air Heater [SAH] is a basic, low-cost, corrosion-free equipment that easily gathers thermal energy from the sun and conveys it to a working medium [5]. At low-temperature gradients, SAHs have been used in commercial ventilation and air conditioning, process heat, agricultural drying, greenhouse dryers, air-water and space heating, distillation, and textile industries [6]. One of the main causes of SAH's low heat transmission is the lower rate of convective coefficient of heat transfer through the air and the roughened absorber plate.

Many studies have given a variety of design configurations with various roughness forms and sizes that have been compared to the smooth kind of SAH to improve SAH Thermo-Hydraulic Performance (THP) [7–9]. To obtain an optimal combination of roughness forms, several experimental investigations [10, 11], numerical simulation and ANN studies [12–14], CFD analysis [15], and thermodynamics correlations [16, 17] incorporating synthetic roughness of various types, shapes, patterns, widths, orientations, rib thickness, and continuity toward flow were conducted [18] Multi-V-ribs with different forms of design parameters configurations like size, shapes, continuity, staggering, and orientation were studied by different research scholars [19, 20] and observed significant improvement in thermos-hydraulic performance.

To study perforation impact on flow characteristics, various studies have been conducted on perforation like for shape-full and half perforation [21], circularity of hole [22, 23], and percentage of open area ratio (β) [24], relative hole location [25]. The open area ratio (β) [26–28] and recirculating frequency [29, 30] were shown to have a substantial influence on Nusselt number fluctuation. Varun et al. [27, 31] studied the effect of perforation in multi-v rib roughened SAH and observed significant improvement in Nu/Nus and THP while keeping a low friction factor.

To obtain an optimal combination of roughness forms and parameters, thermodynamic correlations for SAH were developed by various research scholars. Saini and Saini [32] developed correlations for expanded metal mesh roughened ducts, while Varshney and Saini [33] developed correlations and conducted numerical studies for SAH packed with wire mesh. Both observed significant improvement in THP. Singh et al. [34] established correlations for Nu and f for discrete V-down ribs of roughness installed in SAH. The optimum values of Nu and f were observed to be 3.04 and 3.11 times higher as compared to smooth SAH, respectively. Hans et al. [35] developed correlations for SAH having multiple v-rib roughnesses, the highest values of Nu and f being determined as 6 and 5 times higher as compared to the smooth SAH. The optimum THP was obtained at W/w = 6, whereas the highest f observed at W/w = 10 at α = 60°. Saini and Verma [36] derived correlations for THP for SAH having dimple-shape roughness and improvement in Nu and f values observed as 7.58 and 4.68 times as compared to the smooth channel. Saini and Saini [37] conducted experimental and numerical studies on SAH and developed correlations for Nu and f for SAH with arc-shaped wire roughness and found an improvement of 3.8 times and 1.75 times as compared to smooth SAH. Sethi et al. [38] developed correlations for artificially roughened SAH with dimpled shape roughness and significant improvement in THP. Chamoli and Thakur [39] derived correlations for SAH with perforated baffles having V-shape roughness, while Kumar et al. [40] developed correlations of THP characteristics for 3-sided roughened SAH and Hans et al. [41] derived correlation function for SAH roughened with broken-arc ribs. All three observed improved THP as compared to smooth SAH.

The open area ratio (β) and the recirculation period have both shown a substantial effect on SAH's effectiveness [31]. Varun et al. [26] studied the influence of change in open area ratio (β) and relative roughness width (W/w) in SPSAH with different perforated multi-V rib and observed substantial improvement in performance.

According to a review, perforation in multi-V rib roughness enhances the THP of SAH due to secondary flow developed by holes, resulting in increased turbulence during separation and reattachment [42]. Only a few studies are available with correlation development on impact analysis of variation in β on THP of SAH. Keeping this in mind, the current research further extends Varun et al. [27] work done to analyses the effect of varying β and W/w values and of perforated multi-V rib roughness on THP for the development of correlations for Nu and f as a function of variable parameters of perforated multi-V roughened SPSH.
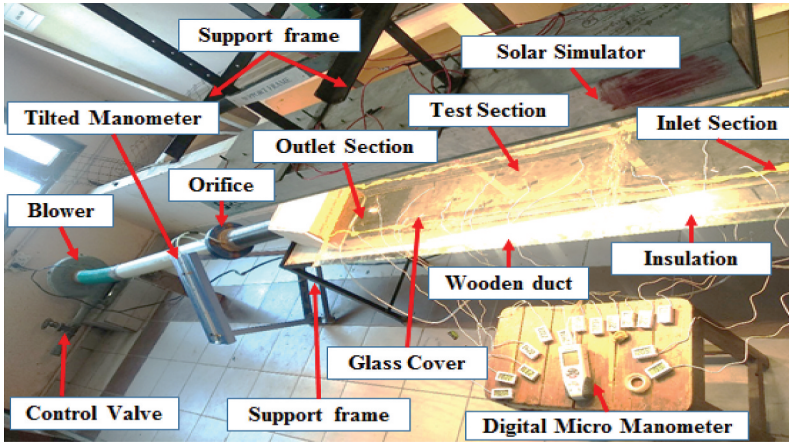
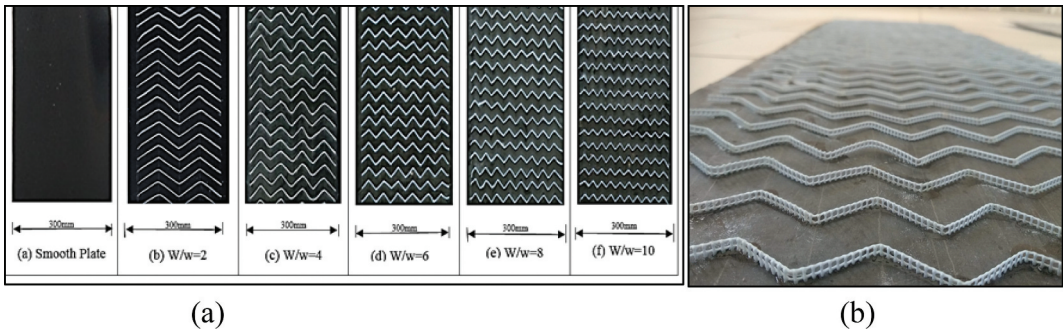**Figure 1.** Experimental setup of SPSAH setup.

Figure 2. (a) Test plate with smooth, W/w = 2, 4, 6, 8, and 10 perforated multi-V rib roughness (b) Perforated-V shape ribs roughness

Setup details

Designed setup configuration and roughness parameters

The ASHRAE standard (AHSRAE 93–77, 1977) was used to create a SAH configuration with perforated multi-V rib roughness as shown in Figure 1. The details of setup configuration and roughness parameters are discussed in a previous study conducted by Varun et al. [27].

The perforated multi-V rib configurations explored in this work are shown in Figure 2. The configuration, range, and values of ribs variables used in the experimental study were derived from existing literature and mentioned in Table 1.

The parameter open area ratio (β) is a ratio of the area of total perforation in the rib and the rib frontal area and can be defined as:

$$\beta = n\left(\pi * \frac{d_h^2}{4}\right)/b * e \tag{1}$$

Where n = number of holes in one rib.

Table 1. Details of parameters used in the experimental investigation.

Parameter with Unit	Value
Width of Duct (W), m	0.3
Elevation of Duct both side (H), m	0.025
Duct aspect ratio (W/H)	12
Relative roughness height (e/D)	0.043
Relative roughness pitch (p/e)	10
The angle of attack (α), in degree	60
Collector slope (β), in degree	0
Relative roughness width (W/w)	2: 4: 6: 8: 10 (five vales)
Open area ratio (β)	0.0(Continuous rib), 0.21, 0.27, 0.31 (four values)
Reynolds Number (Re)	2000:18000 (nine values)
Ribs Type	Multi-V Ribs
Average insolation (I), W/m^{2}	800

Data handling and setup validation

Parameters such as pressure gradient and fluid temperature were gathered for the quasi-state, and the hot air mass flow-rate was estimated using the average airflow temperature and channel pressure difference to explore the impacts of various variables on Nu, f, and THPP. The detailed description of equations associated with data handling, set-up validation and uncertainty analysis were discussed in a previous study conducted by Varun et al. [27].

An experimental set-up of SAH is being used to conduct a validation study, which includes a traditional smooth duct with a Re ranging from 2000 to 18000. Testing findings for Nu and f compared to modified Dittus–Boelter and modified Blasius equations [35], correspondingly as shown in Figure 3.

By using modified Dittus–Boelter equation:

$$Nu_s = 0.024Re^{0.8}Pr^{0.4} \tag{2}$$

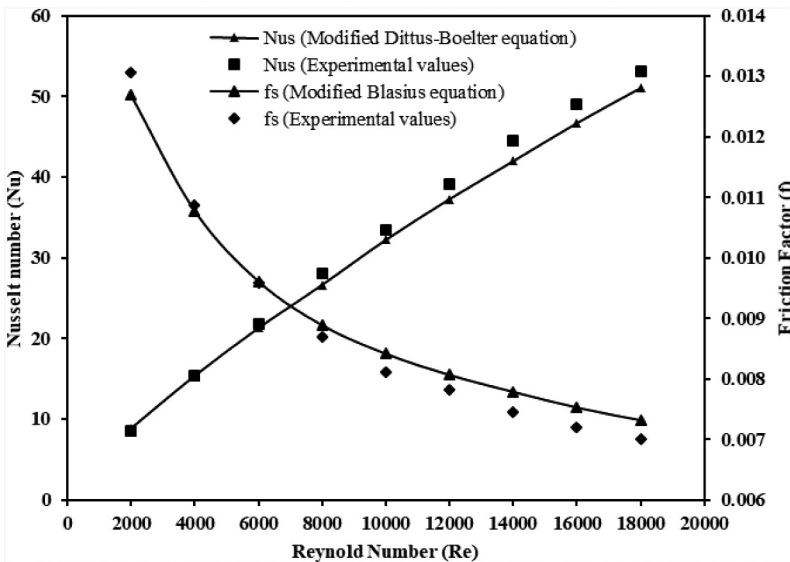By using modified Blasius equation:

$$f_s = 0.085Re^{-0.025} \tag{3}$$

Figure 3. Nus and fs measured and anticipated results for a smooth SAH.

Nu, Re, and f possess maximum percentage errors of ±1.83%, ±1.65%, and ±3.28%, correspondingly.

Results and discussion

The influence of operational and rib variables on flow distribution, THP and mass flow rate is discussed and compared among flat channels for perforated multi-v ribs roughened SPSAH.

Influence of operating parameter

Influence of Reynolds number (Re)

Figure 4(a) shows a comparison of Nu in all cases, indicating a significant gain in Nu at higher values of Re due to a significant reduction in secondary flow and improved mixing and turbulence due to perforation, resulting in a higher Nu and increased thermal performance. The value of Nu observed as 439.80 at W/w = 6 for β = 0.27, at Re = 18000, respectively. Figure 4(b) illustrates a considerable reduction in f attributable to secondary flow created by perforation in multi-V ribs, which lowers fluid stream resistance and saves energy during air circulation. The lowest value of f is 0.0128 for perforated Multi-V Ribs with β = 0.31 at W/w = 2 and Re = 18000. Perforation in Multi-V ribs decreases considerable friction and power usage under the same operating condition.

Influence of relative roughness width (W/w)

Figure 5 shows an initial increase in W/w enhances Nu in all four conditions for the number of variables examined, with the optimal value at W/w = 6. Further increases in the W/w value lower the Nusselt number further. Where as Figure 6 shows that at W/w = 6, fluid mixing caused by roughness attained its optimal values, and a further increase in W/w could obstruct secondary flow formation, leading to a decrease in Nu; the f values continue to rise due to the turbulence formed at high W/w values.

Influence of open area ratio (β)

Figure 7(a) illustrates the influence of β on Nu. This figure shows that Nu is rising as β rises to 0.27, then decreases as a result of the further increase in β value. It can be explained that as the hole diameter gets bigger, the radial development of secondary flow will be stronger for a given axial distance. As an outcome, more fluid mixing takes place in the secondary flow zone, which helps to minimize the flow zone formation on the backside of each rib. It is apparent from this explanation that the β value should be regulated in such a manner that it may enhance the blending of the flow going through the hole to generate local turbulence for enhanced heat transfer among the fluid and the absorber plate. Figure 7 (b) depicts the impact of a change in β value on the f while keeping other parameters same. Because a greater value of β offers less resistance to flow, the f value decreases as the β value increases, resulting in a low f value.

Influence on Nusselt Number ratio (Nu/Nus) and friction factor ratio (f/fs)

Figure 8(a) represents the relationship among Nu/Nus with Re for different perforated multi-V roughness. For all W/w values, the perforated rib with β = 0.27 performs optimally. Further increases in β values lower Nu/Nus, which is reasonable given that fluid mixing induced by roughness achieved its optimal value at β = 0.27 and that a further rise in values might hinder the formation of secondary flow, resulting in a reduction in Nu/Nus values.

The effect of Re on f/fs for different β values is shown in Figure 8(b). The trend demonstrates that when β increases f/fs falls due to the formation of strong secondary flow via the hole.
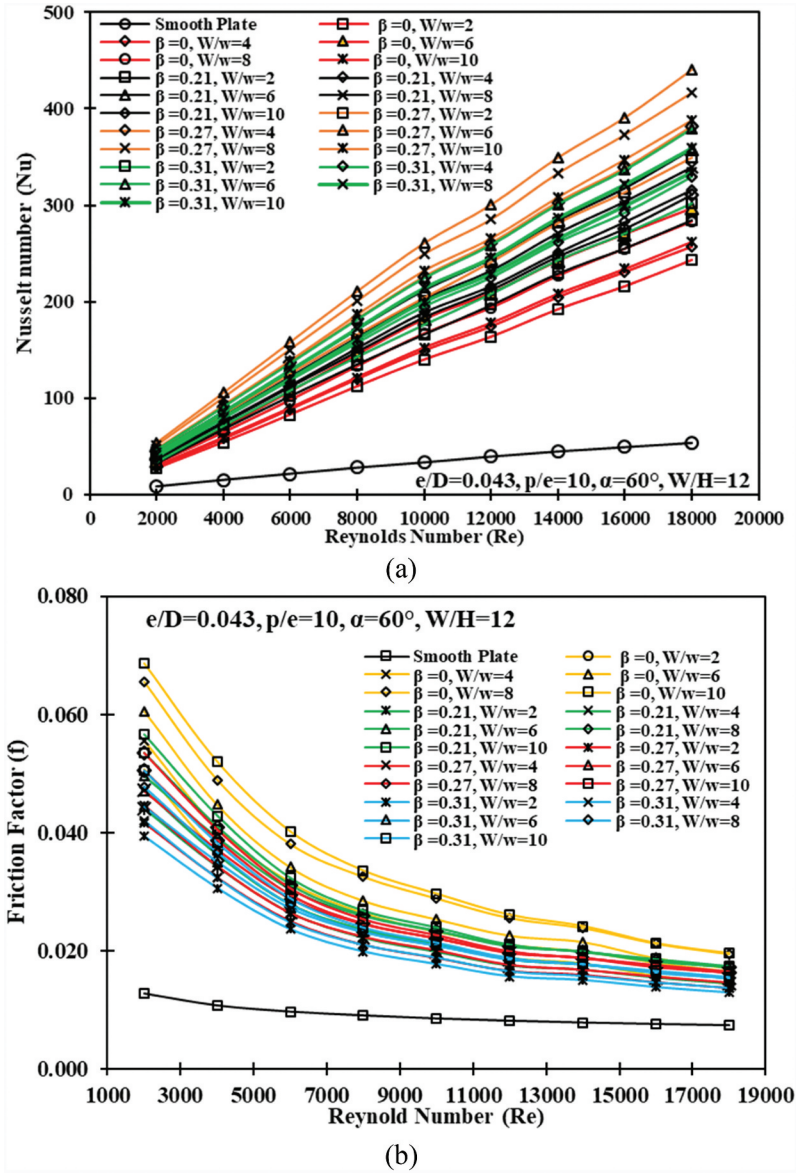
(a)

(b)

Figure 4. Influence of Re on (a) Nu and (b) f values for β = 0.0, β = 0.21, β = 0.27, β = 0.31 at W/w = 6 for perforated multi-V ribs with the smooth channel in SPSAH.

Thermohydraulic performance

The presence of "Nu" and "*f*" generates confusing scenarios in which determining the real benefits of artificial roughness applications looks difficult. Webb and Eckert [43] presented a modified Thermo-Hydraulic Performance Parameter (THPP), designated as THPP and given by equation 4, that refers heat gain to friction loss and assists in evaluating the increase in THP for proposed roughness as compared to the smooth channel for similar energy inputs and defined as:

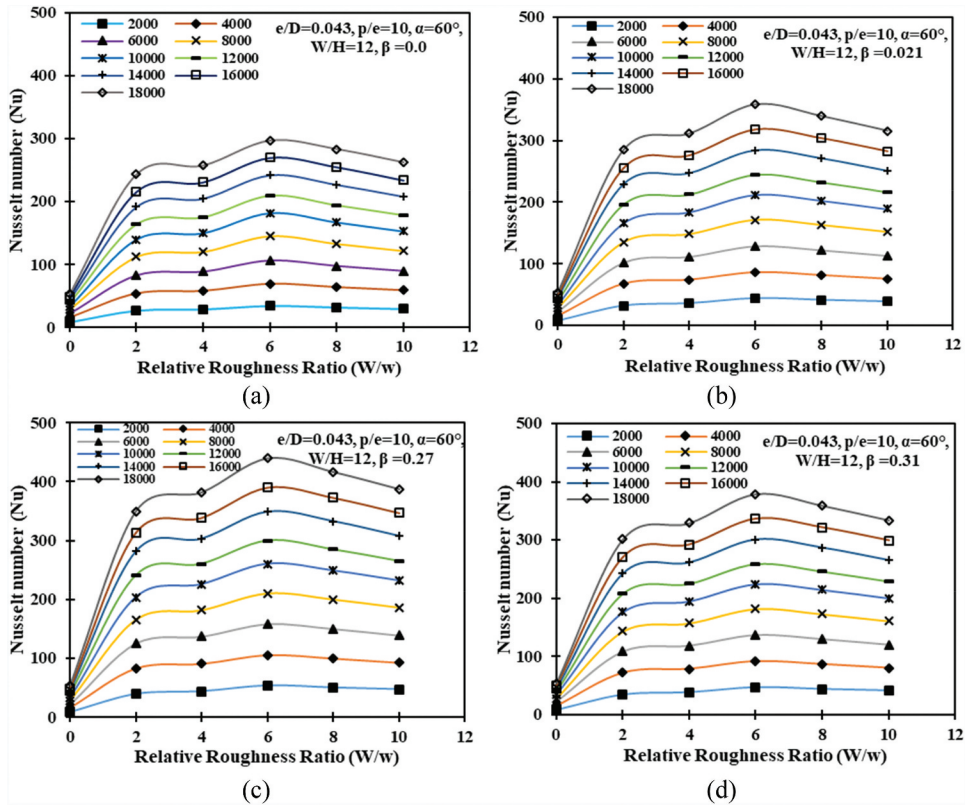$$\text{THPP} = \left[\frac{Nu_r}{Nu_s}\right] / \left[\frac{f_r}{f_s}\right]^{\frac{1}{3}} \tag{4}$$

Figure 5. Influence of W/w on Nu at (a) β = 0.0, (b) β = 0.21, (c) β = 0.27, (d) β = 0.31 at W/w = 6 for a range of different perforated multi-V ribs in SPSAH.

A THPP value higher than one demonstrates the advantages of artificial roughness on smooth plates and may be used to find the best rib patterns for improved THP.

Figure 9(a) presents the connection between THPP and Re for various β values for perforated multi-V ribs in SPSAH, with optimum results obtained for β = 0.27. The optimum value of THPP is 11.08 for β = 0.27 at W/w = 6, respectively. The suggested roughness demonstrates a substantial improvement in THPP values, as compared to the smooth SAH.

Functional relationships for Nusselt number (Nu) and friction factor (f) for SPSAH

For the actual data presented in this study, the statistical correlation between "Nu" and "f" is derived through a regression analysis. The results in the previous sections show that the THPP of artificially roughened SPSAH is a strong function of design and rib geometrical factors [37] like Reynolds number (Re), open area ratio (β), and relative roughness width (W/w). As a result, the functional correlations for Nu and f are as follows:

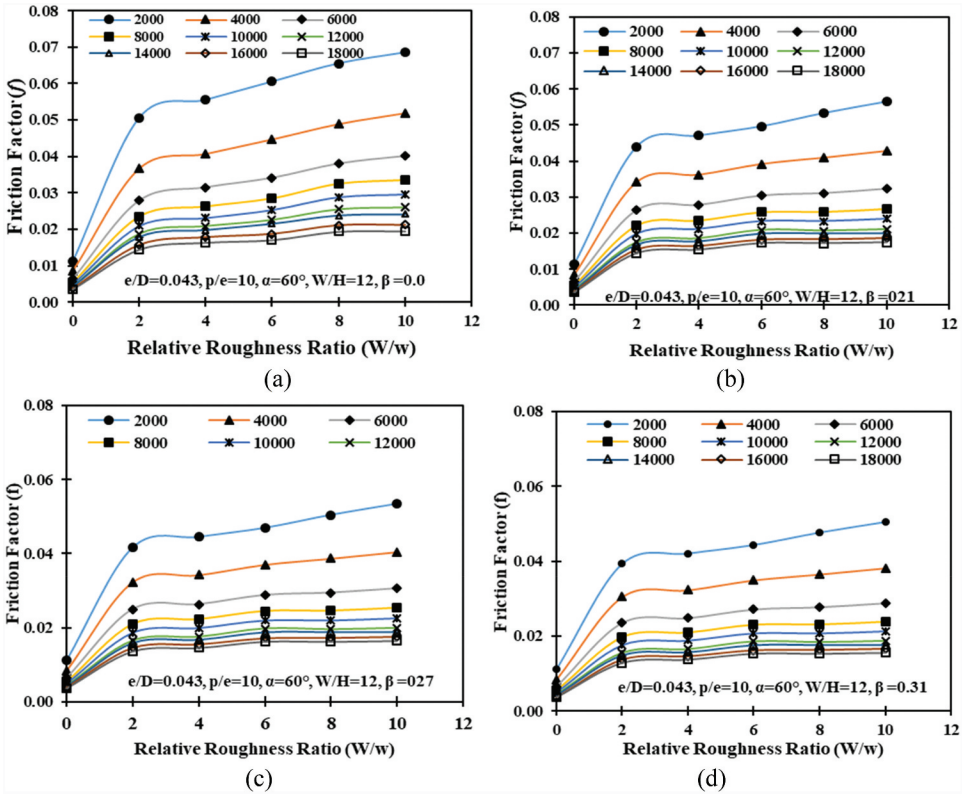$$Nu = (Re, \beta, W/w) \tag{5}$$

$$f = (Re, \beta, W/w) \tag{6}$$

Figure 6. Influence of W/w on f at (a) β = 0.0, (b) β = 0.21, (c) β = 0.27, (d) β = 0.31 at W/w = 6 for a range of different perforated multi-V ribs in SPSAH.
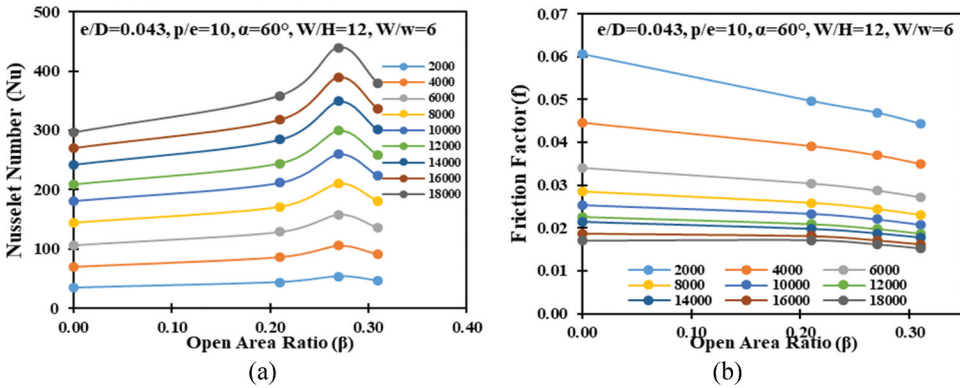

Figure 7. Influence of β on (a) Nu and (b) f values for SPSAH.

Nusselt Number (Nu) correlation

The change in the numeric value of a parameter in connection to other variables would be expressed through correlations. As a result, to obtain Nu correlation, the experimental data set was used in the following manner:

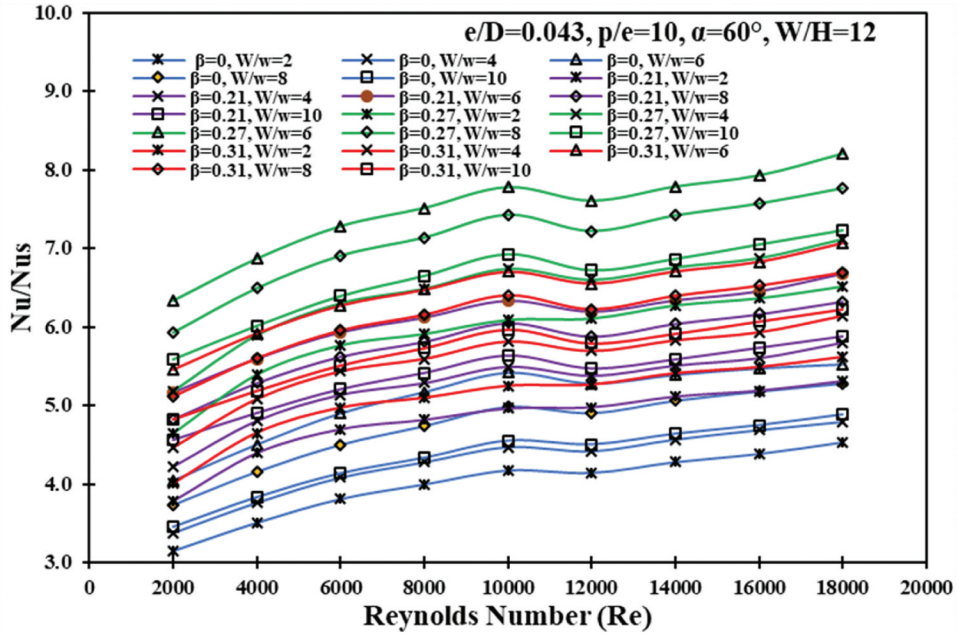- As Re increased, Nu increased monotonically (Figure 4(a)).
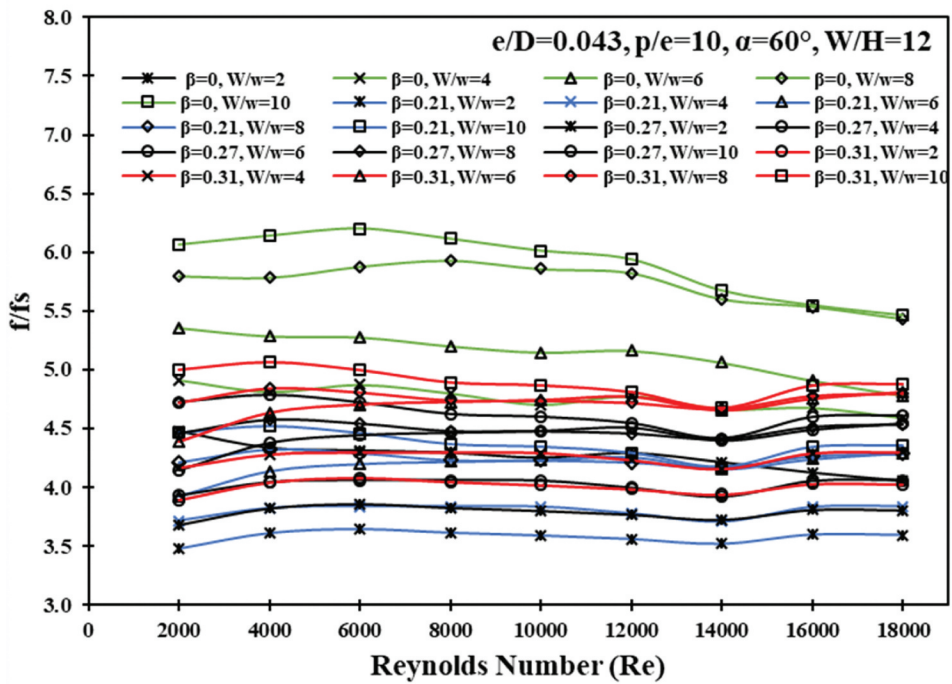
Figure 8. (a) Influence of Re on (a) Nu/Nus values and (b) *f/fs* values at β = 0.0, β = 0.21, β = 0.27, β = 0.31 at W/w = 6 for perforated multi-V ribs in SPSAH
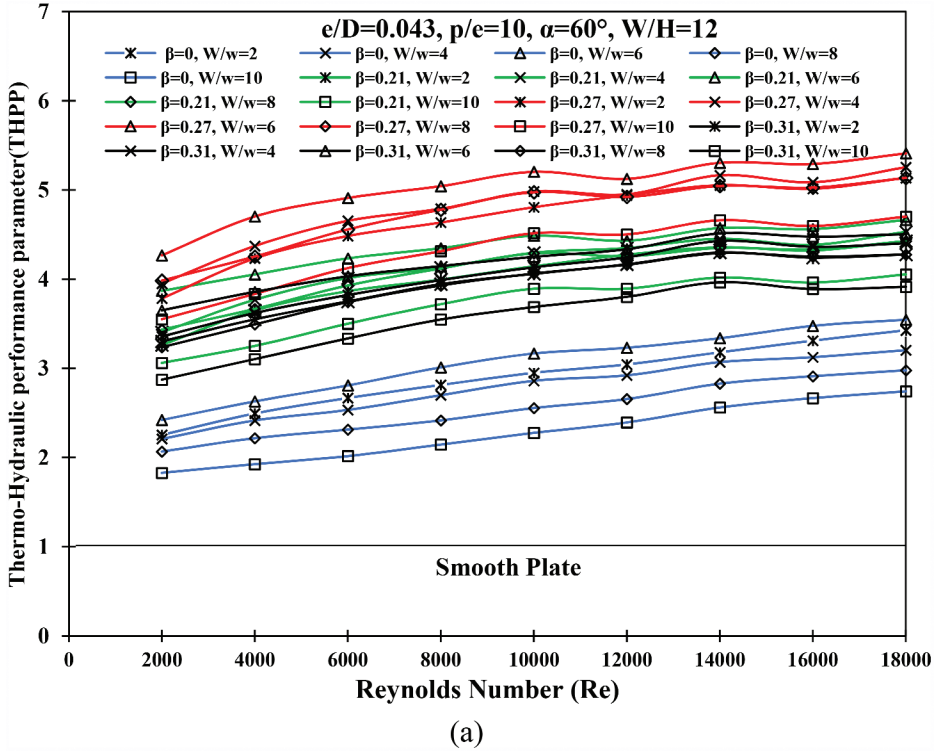
Figure 9. (a) Variation in THPP with Re for different β for perforated multi-V rib in SPSAH

- With increasing W/w value, Nu attain optimum value at W/w = 6 (Figure 5)
- With increasing open area ratio (β), Nu attain maximum value at β = 0.27 (Figure 7(a)).

As a result, the empirical result produces continuous smooth lines including almost uniform slopes (n) with a maximum deviation of 2.37%, but the intercept (A_0) of each line exhibits a wide fluctuation with a maximum deviation of 29.96%, as seen in Figure 10. For the remaining combinations of roughness geometric characteristics, such as W/w and β, identical graphs of the Ln (Nu) vs Ln (Re) have been displayed. Eq. 7 may be used to represent the trends of the line in the plot of Ln (Nu) vs. Ln (Re).
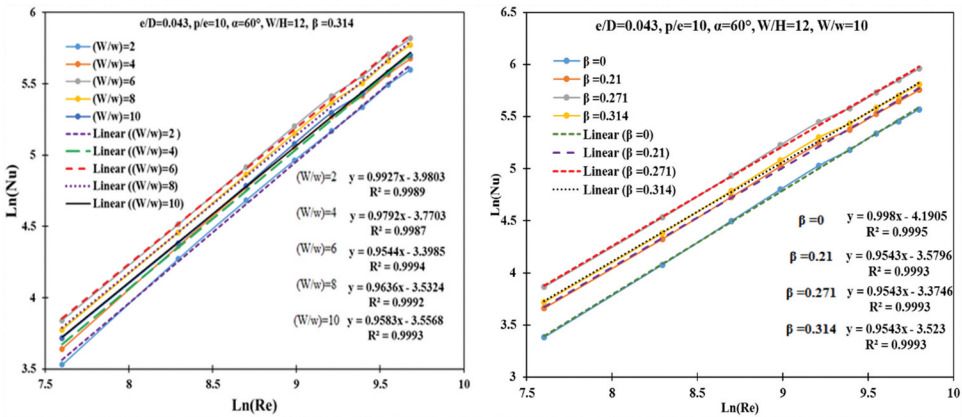

Figure 10. Graph of Ln (Nu) vs Ln (Re) to find out "A_0" and slop "n" for various values of W/w and β in SPSAH.

$$Ln(Nu) = Ln(A_0) + nLn(Re) = A_1 + nLn(Re) \tag{7}$$

Eq.7 can also be written as:

$$Nu = A_0 Re^n \tag{8}$$

Where $A_0 = Anti\ Ln(A_1)$

As illustrated in Figure 11, the least square technique is used to define the appropriate curve throughout the whole range of statistical data sets connected to 21 distinct sets of test runs performed, and the resulting association can be expressed as:

$$Nu = A_0 Re^{0.9648} \tag{9}$$

The value of coefficient A_0 in Eq. 9 for SPSAH is determined by other influencing characteristics such as β and W/w. For SPSAH, to carry out the influence of β on Nu, the value of $A_0 = Nu/(Re)^{0.9648}$ corresponding to all values of W/w and for some specific values of Re has been plotted against relative perforated rib as illustrated in Figure 12. The second-order quadratic equation describes the best fit curve for all the data points. Therefore, regression analysis to fit a second-order polynomial relation on a log–log graph through the data sets is shown in Figure 12, which yields:

$$Ln\left[\frac{Nu}{Re^{0.9648}}\right] = Ln(B_1) + B_2 Ln(\beta) + B_3\ [Ln(\beta)]^2 \tag{10}$$

It can be rearranged as

$$\frac{Nu}{Re^{0.9648}} = B_0(\beta)^{B_2} Exp\left[B_3\ (Ln(\beta))^2\right] \tag{11}$$

Where $B_0 = Anti\ Ln(B_1)$

Substituting the values of B_2, B_3 from the curve fitting results in the following expressions:

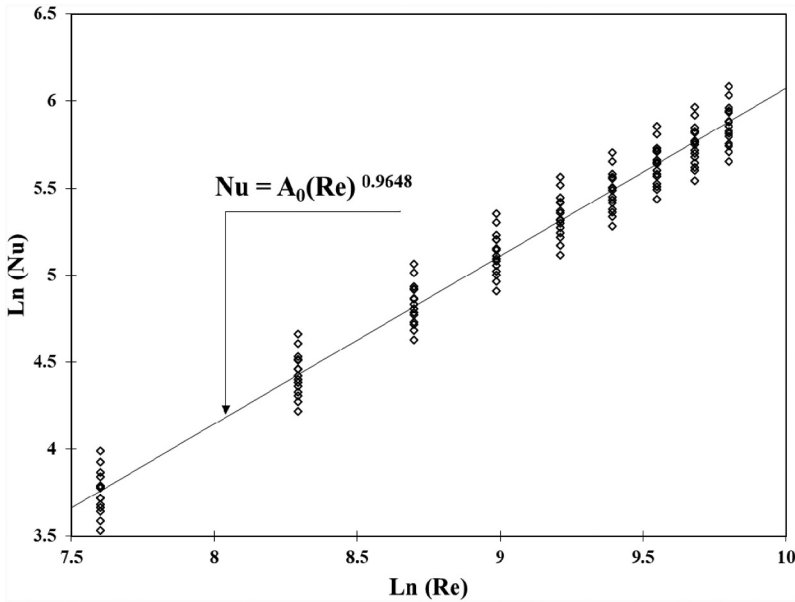$$\frac{Nu}{Re^{0.9648}} = B_0(\beta)^{0.2338} Exp\left[1E^{-12}(Ln(\beta))^2\right] \tag{12}$$

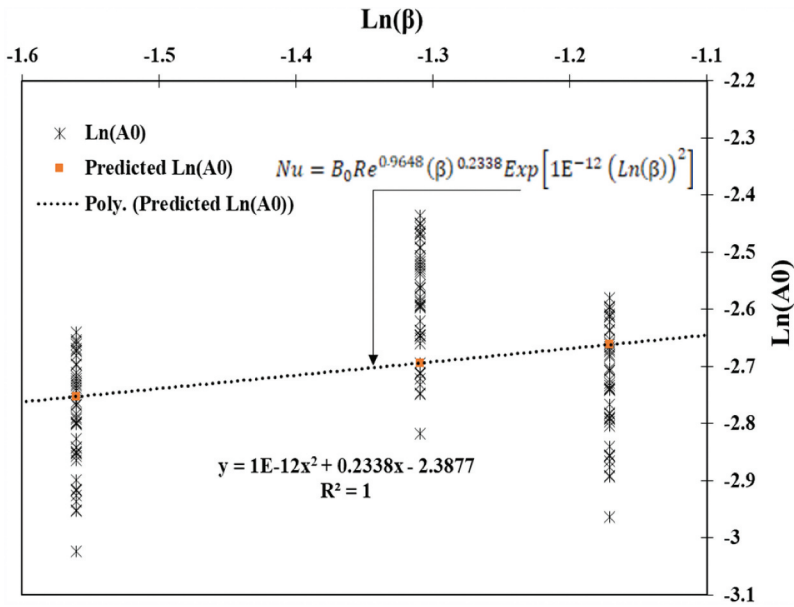**Figure 11.** Ln(Nu) vs Ln(Re) for the entire range of data sets for SPSAH.
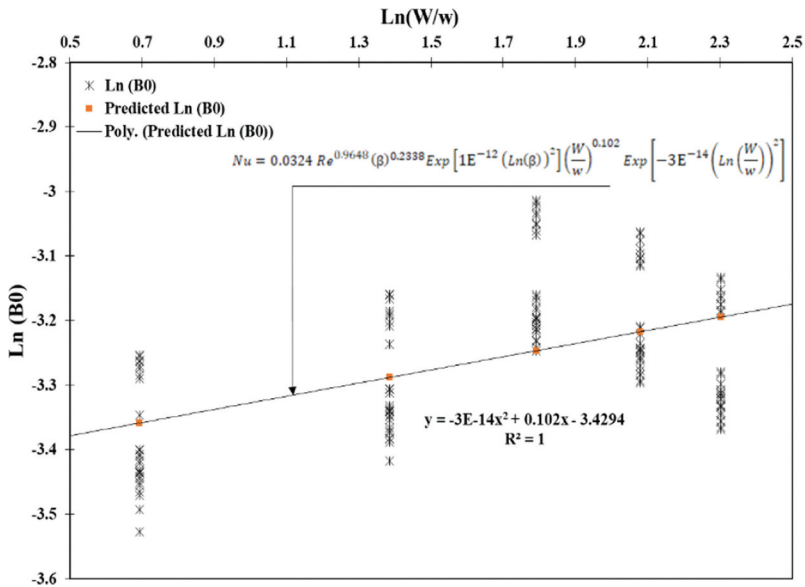
Figure 12. Graph of Ln(A_o) vs. Ln(β) for SPSAH.

Figure 13. Ln(B0) vs. Ln(W/w) for SPSAH.

Different contributing factors influence the coefficient B_0 in Eq.12, namely W/w, and graphing Ln (Nu) vs Ln (W/w) for SPSAH produces the required results. To obtain the functional relationship between Ln (B_0) and Ln (W/w), Figure 13 has been drawn, which shows the second-order polynomial expression to describe the best fit curve. Therefore, considering the parameters W/w the values of $B_0 = \frac{Nu}{Re^{0.9648}(\beta)^{0.2338}Exp\left[1E^{-12}(Ln(\beta))^2\right]}$ have been plotted against W/w in Figure 13. The following second-order polynomial relation has been obtained to best fit the data.

$$Ln\left[\frac{Nu}{Re^{0.9648}(\beta)^{0.2338}Exp\left[1E^{-12}(Ln(\beta))^2\right]}\right] = Ln(C_1) + C_2Ln\left(\frac{W}{w}\right) + C_3\left(Ln\left(\frac{W}{w}\right)\right)^2 \quad (13)$$

This can further be reduced to,

$$\frac{Nu}{Re^{0.9648}(\beta)^{0.2338}Exp\left[1E^{-12}(Ln\beta)^2\right]} = C_0\left(\frac{W}{w}\right)^{C_2}ExpC_3\left(Ln\left(\frac{W}{w}\right)\right)^2 \quad (14)$$

Where $C_0 = $ Anti $Ln(C_1)$

Substituting the values of C_2, C_3 obtained from the regression of the curve fitting gives,

$$\frac{Nu}{Re^{0.9648}(\beta)^{0.2338}Exp\left[1E^{-12}(Ln\beta)^2\right]} = C_0\left(\frac{W}{w}\right)^{0.102}Exp\left[-3E^{-14}\left(Ln\left(\frac{W}{w}\right)\right)^2\right] \quad (15)$$

or

$$Nu = C_0Re^{0.9648}(\beta)^{0.2338}Exp\left[1E^{-12}(Ln\beta)^2\right]\left(\frac{W}{w}\right)^{0.102}Exp\left[-3E^{-14}\left(Ln\left(\frac{W}{w}\right)\right)^2\right] \quad (16)$$

The magnitudes of coefficients $A_0 = 0.02796$, $B_0 = 0.0918$ and $C_0 = 0.0324$ for SPSAH are obtained from fitting the curves in Figure 11 to 13.

The final correlation for Nu can be expressed as:

$$Nu = 0.0324\ Re^{0.9648}(\beta)^{0.2338}Exp\left[1E^{-12}(Ln(\beta))^2\right]\left(\frac{W}{w}\right)^{0.102}Exp\left[-3E^{-14}\left(Ln\left(\frac{W}{w}\right)\right)^2\right] \quad (17)$$

Friction Factor (f) correlation

The same approach was used to calculate the correlation for f as it was for Nu. Friction factor (f), like Nu, was shown to be closely linked to roughness design variables (W/w and β) as well as flow variables (Re). The following is the effect on f values as a function of different roughness variables:

- As Re increased, f decreases monotonically (Figure 4(b)).
- With increasing W/w, f increases and attains a optimum value at W/w = 10 (Figure 6).
- With increasing open area ratio (β), f decreases and attend minimum value at $\beta = 0.31$ (Figure 7 (b)).

Data from the experiments was utilized to do regression analysis, which provided the best fit curve, through which the intercept and slope coefficients for the f correlation were calculated.

The change in f as a function of Re is seen in Figure 14. With empirically collected data, regression analysis was done to obtain the following best-fit curve:

$$Ln(f) = Ln(D_0) + nLn(Re) = D_1 + nLn(Re) \quad (18)$$

$$f = D_0(Re)^{-0.529} \quad (19)$$

Where $D_0 = $ Anti $Ln(D_1)$

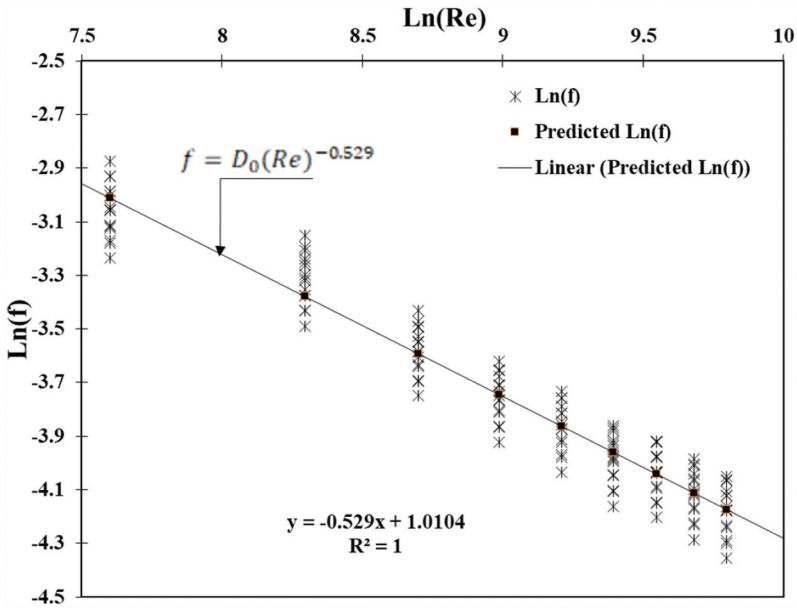**Figure 14.** Graph of Ln(f) as a function of Ln(Re) for all emperical data sets of SPSAH.

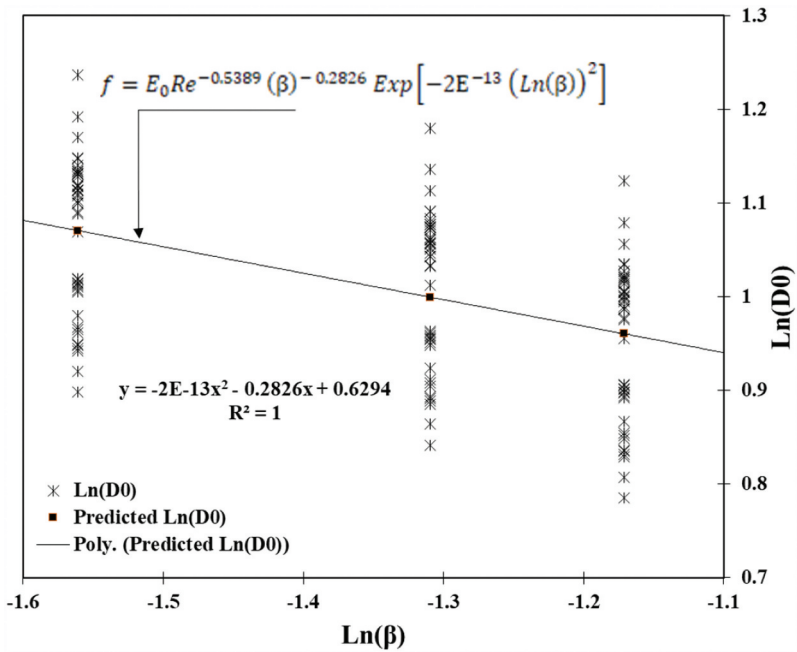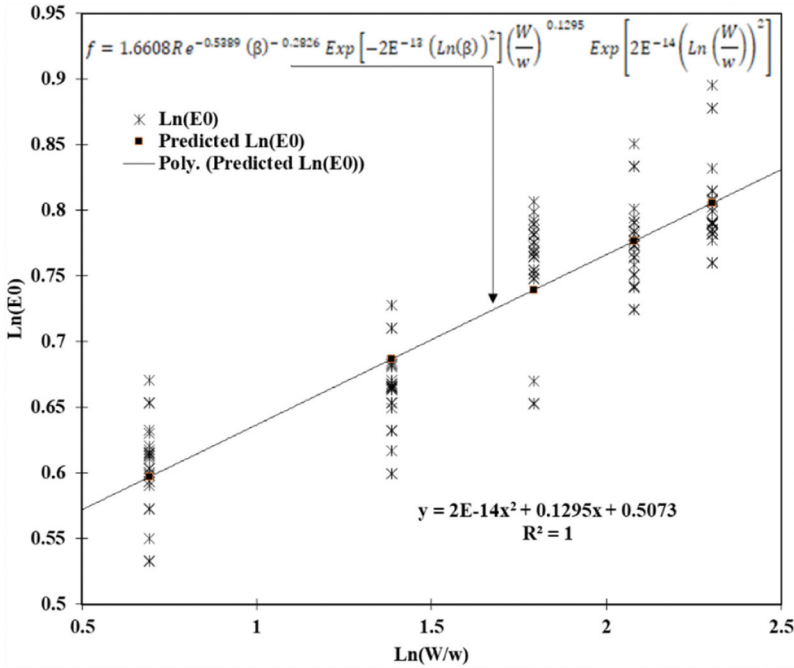**Figure 15.** Graph of Ln(Do) as a function of Ln(β) in case of SPSAH.

Figure 16. Graph of Ln(Eo) as a function of Ln(W/w) in case of SPSAH.

For SPSAH, the coefficient D_0 is as a result of other contributing factors as, β, and W/w. To bring out the effect of the values of $D_0 = \frac{f}{Re^{-0.529}}$ corresponding to all values of open area ratio (β) are plotted against perforated multi-V rib as shown in Figure 15, that shows a regression technique to draw a second-order polynomial curve on a log–log graph across the data sets. can be express as:

$$Ln\left[\frac{f}{Re^{-0.529}}\right] = Ln(E_1) + E_2 Ln(\beta) + E_3[Ln(\beta)]^2 \tag{20}$$

It can be rearranged as,

$$\frac{f}{Re^{-0.529}} = E_0(\beta)^{E_2} Exp\left[E_3(Ln(\beta))^2\right] \tag{21}$$

Where E_0 = Anti Ln(E_1)

Substituting the values of E_2, E_3 from the curve fitting results in the following expressions;

$$\frac{f}{Re^{-0.529}} = E_0(\beta)^{E_2} Exp\left[E_3 \ (Ln(\beta))^2\right] \tag{22}$$

Or

$$\frac{f}{Re^{-0.529}} = E_0(\beta)^{-0.2826} Exp\left[-2E^{-13} \ (Ln(\beta))^2\right] \tag{23}$$

The coefficient E_0 in Eq. 23 is a result of other contributing variables, namely W/w, and the desired plots can be obtained by plotting Ln (f) vs Ln (W/w) for SPSAH. To obtain the functional relationship between Ln(B_0) and Ln (W/w), Figure 16 has been drawn, which shows the second-order polynomial expression to describe the best fit curve. Therefore, considering the parameters W/w the values of $E_0 = \frac{f}{Re^{-0.529}(\beta)^{-0.2826} Exp\left[-2E^{-13} \ (Ln(\beta))^2\right]}$ have been plotted against W/w in Figure 16.

The following second-order polynomial relation has been obtained to best fit the data.

$$Ln\left[\frac{f}{Re^{-0.529}(\beta)^{-0.2826}\,Exp\left[-2E^{-13}\,(Ln(\beta))^2\right]}\right] = Ln(F_1) + F_2 Ln\left(\frac{W}{w}\right) + F_3\left(Ln\left(\frac{W}{w}\right)\right)^2 \quad (24)$$

This can further be reduced to,

$$\frac{f}{Re^{-0.529}(\beta)^{-0.2826}\,Exp\left[-2E^{-13}\,(Ln\beta)^2\right]} = F_0\left(\frac{W}{w}\right)^{F_2} Exp\left[F_3\left(Ln\left(\frac{W}{w}\right)\right)^2\right] \quad (25)$$

Where F_0 = Anti Ln (F_1)

Substituting the values of F_2 and F_3 obtained from the regression of the curve fitting gives,

$$\frac{f}{Re^{-0.529}(\beta)^{-0.2826}\,Exp\left[-2E^{-13}\,(Ln\beta)^2\right]} = F_0\left(\frac{W}{w}\right)^{0.1295} Exp\left[-9E-15\left(Ln\left(\frac{W}{w}\right)\right)^2\right] \quad (26)$$

$$f = F_0 Re^{-0.529}(\beta)^{-0.2826}\,Exp\left[-2E^{-13}\,(Ln\beta)^2\right]\left(\frac{W}{w}\right)^{0.1295} Exp\left[2E^{-14}\left(Ln\left(\frac{W}{w}\right)\right)^2\right] \quad (27)$$

The values of coefficients D_0 = 2.7469, E_0 = 1.876 and F_0 = 1.6608 for SPSAH are obtained from fitting the curves in Figure 14 to 16.

The final correlation for f can be expressed as:

$$f = 1.6608 Re^{-0.529}(\beta)^{-0.2826}\,Exp\left[-2E^{-13}\,(Ln(\beta))^2\right]\left(\frac{W}{w}\right)^{0.1295} Exp\left[2E^{-14}\left(Ln\left(\frac{W}{w}\right)\right)^2\right] \quad (28)$$
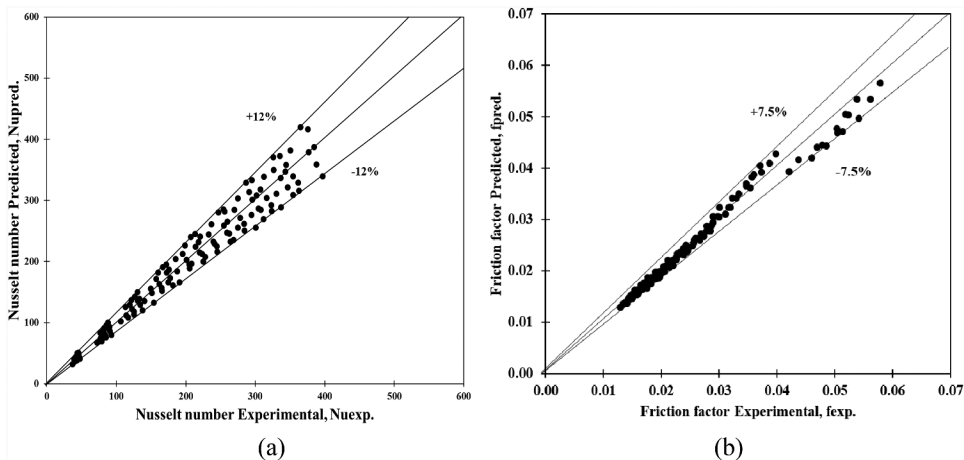

Figure 17. Comparison of empirical and projected results of (a) Nu (b) f for developed correlation for SPSAH.

Deviation in theoretical and experimental Nusselt number (Nu) and friction factor (f)

Figure 17(a,b) compares empirical Nu and f data with predicted Nu and f projections and signifies that approximately 98% of the data points are located within ± 12% and ±7.5% deviation lines with regression coefficient (R[2]) of the correlations are 0.95 and 0.96, respectively. As a result, the established correlation equations (17) and (28) may be implemented to forecast the Nu and f within acceptable ranges for the parameters studied in this study.

Conclusions

The THP and correlation studies in a SPSAH duct with different perforated multi-V ribs exposed to an equally distributed thermal gradient of radiant heat demonstrate that perforated multi-V ribs significantly boost THP. The following are the findings obtained from the aims of the present study:

- The optimum performance of perforated multi-V rib roughness was found with an open area ratio (β) of 0.27 in all cases.
- The value of Nu attained its optimal value at W/w = 6, while the f value increases as W/w increases.
- The highest improvement in Nu/Nus and f/fs as compared to smooth channels was found 8.19 times and 4.78 times, respectively.
- The optimum value of THPP was observed as 5.41 for perforated multi-V rib roughness with an open area ratio (β) of 0.27.
- Within the pre-defined range of parameters W/w, β and Re, correlations for Nu and f developed with ±12% and ±7.5% of forecasting, respectively.

As shown in this study, the optimal value of the open area ratio for perforated multi-V ribs improves thermos-hydraulic performance significantly when compared to a smooth duct. Hence, the improved findings indicate the possibility of using perforation in various ribs in artificially roughened SAH. Further study can also be applied to double-pass solar air heaters with various rib roughness.

Acknowledgments

Disclosure statement

No potential conflict of interest was reported by the authors.

ORCID

Varun Pratap Singh 🆔 http://orcid.org/0000-0002-2148-5604
Siddharth Jain 🆔 http://orcid.org/0000-0002-0579-2823

Nomenclature

Details of symbols	Dimensionless parameters
D_h Duct hydraulic diameter, (m)	e/D_h Relative roughness height
e Elevation of rib, (m)	f duct friction
H Elevation of channel/duct, (m)	Nu Roughened plate Nusselt number

(Continued)

Details of symbols	Dimensionless parameters
$\dot{m}$ Air mass-flow rate, (kg/s)	P/e Relative roughness pitch
W Width of duct channel, (m)	Re Reynolds number
w Width of one set of rib, (m)	W/H Channel aspect ratio
Abbreviations	W/w Relative roughness width
CFD Computational Fluid Dynamics	*Greek symbols*
THP Thermo-Hydraulic Performance	α Angle of attack, (°)
SPSAH Single Pass Solar Air Heater	β Collector slope, the open area ratio

References

[1] S. Jain and M. P. Sharma, "Oxidation, thermal, and storage stability studies of jatropha curcas biodiesel," *International Scholarly Research Notices*, vol. 2012, 2012. DOI: 10.5402/2012/861293.

[2] P. Goyal, M. P. Sharma, and S. Jain, "Optimization of transesterification of jatropha curcas oil to biodiesel using response surface methodology and its adulteration with kerosene," *J. Mater. Environ. Sci.*, vol. 4, no. 2, pp.277–284, 2013.

[3] S. Jain and M. P. Sharma, "Engine performance and emission analysis using oxidatively stabilized Jatropha curcas biodiesel," *Fuel*, vol. 106, pp. 152–156, 2013. DOI: 10.1016/j.fuel.2012.11.076.

[4] V. P. Singh, M. Saini, A. Sharma, S. Jain, and G. Dwivedi, "Solar thermal receivers — a review," *Lect. Notes Mech. Eng*, vol. II, pp. 1–25, 2022. DOI: 10.1007/978-981-16-8341.

[5] R. K. Ravi and R. P. Saini, "Experimental investigation on performance of a double pass artificial roughened solar air heater duct having roughness elements of the combination of discrete multi V shaped and staggered ribs," *Energy*, vol. 116, pp. 507–516, 2016. DOI: 10.1016/j.energy.2016.09.138.

[6] T. Alam and M. H. Kim, "A critical review on artificial roughness provided in rectangular solar air heater duct," *Renew. Sustain. Energy Rev*, vol. 69, pp. 387–400, July. 2016. 2017. DOI: 10.1016/j.rser.2016.11.192.

[7] B. Kumar, A. K. Patil, S. Jain, and M. Kumar, "Study of entropy generation in heat exchanger tube with multiple V cuts in perforated twisted tape insert," *J. Heat Transfer*, vol. 141, no. August, pp. 1–8, 2019. DOI: 10.1115/1.4043769.

[8] B. Kumar, M. Kumar, A. K. Patil, and S. Jain, "Effect of V cut in perforated twisted tape insert on heat transfer and fluid flow behavior of tube flow : an experimental study," *Exp. Heat Transf*, pp. 1–21, 2018. DOI: 10.1080/08916152.2018.1545808.

[9] T. Alam, R. P. Saini, and J. S. Saini, "Experimental investigation of thermohydraulic performance of a rectangular solar air heater duct equipped with V-shaped perforated blocks," *Adv. Mech. Eng*, vol. 2014, 2014. DOI: 10.1155/2014/948313.

[10] G. K. Chhaparwal, A. Srivastava, and R. Dayal, "Artificial repeated-rib roughness in a solar air heater – a review," *Sol. Energy*, vol. 194, no. August, pp. 329–359, 2019. DOI: 10.1016/j.solener.2019.10.011.

[11] S. Meena, C. S. Meena, and V. K. Bajpai, "Thermal performance of flat-plate collector : an experimental study," March, pp. 1–4. 2014.

[12] A. S. Yadav and S. K. Sharma, "Numerical simulation of ribbed solar air heater," *Advances in Fluid and Thermal Engineering*, pp. 549–558, 2021. DOI: 10.1007/978-981-16-0159-0_49.

[13] A. S. Yadav, *et al.*, "Enhanced solar thermal air heater: a numerical investigation," *Mater. Today Proc*, vol. 47, no. xxxx, pp. 2777–2783, 2021. DOI: 10.1016/j.matpr.2021.03.385.

[14] T. Alam, C. S. Meena, N. B. Balam, A. Kumar, and R. Cozzolino, "Thermo-hydraulic performance characteristics and optimization of protrusion rib roughness in solar air heater," *Energies*, vol. 14, no. 11, pp. 3159, 2021. DOI: 10.3390/en14113159.

[15] M. Sharma, D. E. Kumari, and D. P. Meena, "CFD analysis in solar air heater for heat transfer enhancement: a review," *SSRN Electron. J*, no. June, 2021. DOI: 10.2139/ssrn.3809706.

[16] R. Prasad, A. S. Yadav, N. K. Singh, and D. Johari, "Heat transfer and friction characteristics of an artificially roughened solar air heater BT," *Advances in fluid and thermal engineering*, pp. 613–626, 2019.

[17] C. S. Meena, S. Meena, and V. K. Bajpai, "Correlation between absorber plate thickness δ and collector efficiency factor F' of solar flat-plate collector," *Appl. Mech. Mater*, vol. 592–594, pp. 2341–2344, 2014. 10.4028/www.scientific.net/AMM.592-594.2341 .

[18] T. Alam, *et al.*, "Performance augmentation of the flat plate solar thermal collector: a review," *Energies*, vol. 14, no. 19, pp. 6203, Sep. 2021. DOI: 10.3390/en14196203.

[19] B. Kumar, A. K. Patil, S. Jain, and M. Kumar, "Effects of double V cuts in perforated twisted tape insert: an experimental study," *Heat Transf. Eng*, vol. 41, no. 17, pp. 1473–1484, 2020. DOI: 10.1080/01457632.2019.1649926.

[20] A. Kumar and A. Layek, "Evaluation of the performance analysis of an improved solar air heater with winglet shaped ribs," *Exp. Heat Transf*, pp. 1–19, 2020. DOI: 10.1080/08916152.2020.1838670.

[21] R. Karwa and B. K. Maheshwari, "Heat transfer and friction in an asymmetrically heated rectangular duct with half and fully perforated baffles at different pitches," *Int. Commun. Heat Mass Transf*, vol. 36, no. 3, pp. 264–268, 2009. DOI: 10.1016/j.icheatmasstransfer.2008.11.005.

[22] J. S. Kwak and S. Shin, "Effect of hole shape on the heat transfer in a rectangular duct with perforated blockage walls," *J. Mech. Sci. Technol*, vol. 22, no. April, pp. 1945–1951, 2008. DOI: 10.1007/s12206-008-0736-7.

[23] T. Alam, R. P. Saini, and J. S. Saini, "Effect of circularity of perforation holes in V-shaped blockages on heat transfer and friction characteristics of rectangular solar air heater duct," *Energy Convers. Manag*, vol. 86, pp. 952–963, 2014. DOI: 10.1016/j.enconman.2014.06.050.

[24] T. Alam, R. P. Saini, and J. S. Saini, "Experimental investigation on heat transfer enhancement due to V-shaped perforated blocks in a rectangular duct of solar air heater," *Energy Convers. Manag*, vol. 81, pp. 374–383, 2014. DOI: 10.1016/j.enconman.2014.02.044.

[25] S. Chamoli and N. S. Thakur, "Heat transfer enhancement in solar air heater with V-shaped perforated baffles," *J. Renew. Sustain. Energy*, vol. 5, no. 2, pp. 023122, 2013. DOI: 10.1063/1.4798411.

[26] V. P. Singh, S. Jain, and J. M. L. Gupta, "Analysis of the effect of variation in open area ratio in perforated multi-V rib roughened single pass solar air heater- part A," *Energy Sources, Part A Recover. Util. Environ. Eff*, pp. 1–20, 2022. DOI: 10.1080/15567036.2022.2029976.

[27] S. Jain, J. Gupta, and V. P. Singh, "Analysis of the effect of perforation in multi-v rib artificial roughened single pass solar air heater: - part A," *Exp. Heat Transf*, pp. 1–20, Oct. 2021. DOI: 10.1080/08916152.2021.1988761.

[28] S. Jain, J. Gupta, and V. P. Singh, "Performance assessment of double-pass parallel flow solar air heater with perforated multi-V ribs roughness — part B," *Exp. Heat Transf*, pp. 1–18, 2022. DOI: 10.1080/08916152.2021.2019147.

[29] J. Liu, *et al.*, "Heat transfer enhancement and turbulent flow in a rectangular channel using perforated ribs with inclined holes," *J. Heat Transfer*, vol. 141, no. 4, 2019. DOI: 10.1115/1.4042841.

[30] A. Kumar, N. Kumar, S. Kumar, and R. Maithani, "Exergetic efficiency analysis of impingement jets integrated with internal conical ring roughened solar heat collector," *Exp. Heat Transf*, pp. 1–21, Nov. 2021. DOI: 10.1080/08916152.2021.2002466.

[31] A. Tariq, P. K. Panigrahi, and K. Muralidhar, "Flow and heat transfer in the wake of a surface-mounted rib with a slit," *Exp. Fluids*, vol. 37, no. 5, pp. 701–719, 2004. DOI: 10.1007/s00348-004-0861-8.

[32] R. P. Saini and J. S. Saini, "Heat transfer and friction factor correlations for artificially roughened ducts with expanded metal mesh as roughness element," *Int. J. Heat Mass Transf*, vol. 40, no. 4, pp. 973–986, 1996. DOI: 10.1016/0017-9310(96)00019-1.

[33] L. Varshney and J. S. Saini, "Heat transfer and friction factor correlations for rectangular solar air heater duct packed with wire mesh screen matrices," *Sol. Energy*, vol. 62, no. 4, pp. 255–262, 1998. DOI: 10.1016/S0038-092X (98)00017-6.

[34] S. Singh, S. Chander, and J. S. Saini, "Heat transfer and friction factor correlations of solar air heater ducts artificially roughened with discrete V-down ribs," *Energy*, vol. 36, no. 8, pp. 5053–5064, 2011. DOI: 10.1016/j.energy.2011.05.052.

[35] V. S. Hans, R. P. Saini, and J. S. Saini, "Heat transfer and friction factor correlations for a solar air heater duct roughened artificially with multiple v-ribs," *Sol. Energy*, vol. 84, no. 6, pp. 898–911, 2010. DOI: 10.1016/j.solener.2010.02.004.

[36] R. P. Saini and J. Verma, "Heat transfer and friction factor correlations for a duct having dimple-shape artificial roughness for solar air heaters," *Energy*, vol. 33, no. 8, pp. 1277–1287, 2008. DOI: 10.1016/j.energy.2008.02.017.

[37] S. K. Saini and R. P. Saini, "Development of correlations for nusselt number and friction factor for solar air heater with roughened duct having arc-shaped wire as artificial roughness," *Sol. Energy*, vol. 82, no. 12, pp. 1118–1130, 2008. DOI: 10.1016/j.solener.2008.05.010.

[38] M. Sethi,Varun, N. S. Thakur, and N. S. Thakur, "Correlations for solar air heater duct with dimpled shape roughness elements on absorber plate," *Sol. Energy*, vol. 86, no. 9, pp. 2852–2861, Sep. 2012. DOI: 10.1016/j.solener.2012.06.024.

[39] S. Chamoli and N. S. Thakur, "Correlations for solar air heater duct with V-shaped perforated baffles as roughness elements on absorber plate," *Int. J. Sustain. Energy*, vol. 35, no. 1, pp. 1–20, 2016. DOI: 10.1080/14786451.2013.857318.

[40] A. Kumar, B. N. Prasad, and K. D. P. Singh, "Development of correlations of heat transfer and fluid flow characteristics for three sides artificially roughened solar air heaters," *J. Heat Mass Transf*, vol. 15, no. 1, pp. 93–123, 2018. DOI: 10.17654/HM015010093.

[41] V. S. Hans, R. S. Gill, and S. Singh, "Heat transfer and friction factor correlations for a solar air heater duct roughened artificially with broken arc ribs," *Exp. Therm. Fluid Sci*, vol. 80, pp. 77–89, 2017. DOI: 10.1016/j. expthermflusci.2016.07.022.

[42] T. Alam and M. H. Kim, "A critical review on artificial roughness provided in rectangular solar air heater duct". *Renew. Sustain. Energy Rev*, vol. 69, no. October, pp. 387–400, 2016, 2017. DOI: 10.1016/j. rser.2016.11.192.

[43] E. R. G. E. R. L. WEBB and E. R. G. Eckert, "Application of rough surfaces to heat exchanger," *Int. J. Heat Mass Transf*, vol. 15, no. 9, pp. 1647–1658, 1972. DOI: 10.1016/0017-9310(72)90095-6.